RSC Advances

This is an *Accepted Manuscript*, which has been through the Royal Society of Chemistry peer review process and has been accepted for publication.

Accepted Manuscripts are published online shortly after acceptance, before technical editing, formatting and proof reading. Using this free service, authors can make their results available to the community, in citable form, before we publish the edited article. This *Accepted Manuscript* will be replaced by the edited, formatted and paginated article as soon as this is available.

You can find more information about *Accepted Manuscripts* in the **Information for Authors**.

Table of Contents Graphic and Synopsis

Highly reduced phosphomolybdates are catalytically active for electron transfer reaction of Ferricyanide to Ferrocyanide.
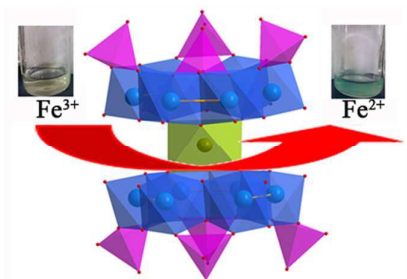
Journal Name

ARTICLE

Manganese-Phosphomolybdate Molecular Catalyst for Electron Transfer Reaction of Ferricyanide to Ferrocyanide

Kaining Gong, Yunping Liu, and Zhangang Han*

Three manganese-containing phosphomolybdate hybrids $(H_2bpp)_5[Na(Hbpp)]_6H_{10}\{Mn[Mo_6O_{12}(OH)_3(HPO_4)_4]_2\}_4\cdot14H_2O$ (**1**), $Na_4(H_2bpp)_2[Mn(H_2O)_7]\{Mn[Mo_6O_{12}(OH)_3(HPO_4)_3(PO_4)]_2\}\cdot2H_2O$ (**2**), $Na(H_2O)_2(Hbpp)_3[Na_2(bpp)(H_2O)][Mn_2(H_2O)_5]-\{Mn[Mo_{12}O_{24}(OH)_6(HPO_4)_6(H_2PO_4)(PO_4)]\}\cdot(HPO_4)\cdot H_2O$ (**3**) (bpp = 1,3-bi(4-pyridyl)-propane), had been constructed and characterized. In three hybrids, the inorganic moieties consist of a 'hourglass-shape' anionic cluster which is composed of two reduced polymolybdenum phosphate $[P^V_4Mo^V_6O_{28}(OH)_3]_9\{P_4Mo_6\}$ units bridged by one manganese ion. The preliminary experiments show that these hybrids as a unique class of molecular catalysts are highly active for promoting the inorganic electron transfer (redox) reaction of ferricyanide to ferrocyanide by thiosulphate with high rate constants under mild condition. These catalysts with the structural identity maintained both in solutions and solid state can be easily separated from the reaction solution for the next cycle catalytic reaction.

1. Introduction

In recent years, researchers have been great concerns on metal nanoparticles (NPs) because of the special nature and in many application fields, such as catalysis, photonics, electronics, biomedicine and biosensors.[1-8] The major disadvantages of using metal NPs as catalysts are in their aggregation during the catalytic process and separation after the end of reaction (which also causes loss). These problems cause severe restrictions in using costly metal NPs as catalysts for large scale applications. So searching for new materials-based catalysts with the structural stability, as well as easy separation and good reusability for several cycles, are ongoing. Recently, metal NPs embedded in mesoporous hosts in the form of powder/bulk showed some improvements,[9-10] however, the separation and reuse of catalysts were still a tough issue. The pursuit of more environmentally friendly and economical catalytic systems is still the most important work as well as a challenge.

Polyoxometalates (POMs) as a kind of important inorganic building blocks with special and stable nanoscale structures have been used to construct novel hybrid materials with specific properties. As one important polyanion in POM family, phosphomolybdates $\{P_4Mo_6X_{31}\}$(X= O or OH) units (abbreviated as $\{P_4Mo_6\}$) have attracted a great deal of attentions of researchers due to their unique reduced structural feature.[11-16] It is well known that the significant property of POMs is their ability to reversibly accept several electrons and therefore to act as electron reservoirs. The unique reduced structure of $\{P_4Mo_6\}$ with d^1 electronic conformation of Mo^V can be expected to apply in electron transfer reaction catalysts. Our recent research has focused on POM-based supramolecular assemblies by utilizing the noncovalent weak forces that occur between the surface oxygen atoms of POMs and organic molecules.[17-22] A feature is in that these hybrids have good structural stability in water and common organic solvents, which provides the convenience for application in heterogenous catalyst. With these considerations in the head, three functional analogs[23] have been isolated. Their formula are: $(H_2bpp)_5[Na(Hbpp)]_6H_{10}\{Mn[Mo_6O_{12}-(OH)_3(HPO_4)_4]_2\}_4\cdot14H_2O$ (**1**), $Na_4(H_2bpp)_2[Mn(H_2O)_7]-\{Mn[Mo_6O_{12}(OH)_3(HPO_4)_3(PO_4)]_2\}\cdot2H_2O$ (**2**), $Na(H_2O)_2(Hbpp)_3-[Na_2(bpp)(H_2O)][Mn_2(H_2O)_5]\{Mn[Mo_{12}O_{24}(OH)_6(HPO_4)_6(H_2PO_4)-(PO_4)]\}\cdot(HPO_4)\cdot H_2O$ (**3**) (bpp = 1,3-bi(4-pyridyl)-propane). Experimental results indicate that hybrids **1-3** are highly active molecular catalysts for promoting the inorganic electron transfer (redox) reaction of ferricyanide to ferrocyanide by thiosulphate. Since this class of hybrids is insoluble in the reaction medium, the catalysts can be easily filtered after the reaction is completed. the stability and reusability of these hybrids is also investigated.

2. Experimental section

2.1 Materials and measurements

All the reagents were commercially purchased and used without further purification. Hydrothermal synthesis was carried out with a 20 mL Teflon-lined autoclave under autogenous pressure. The reaction vessels were filled to approximately 70% of their volume capacity. Elemental analysis of C, H, N were carried on a Perkin-Elmer 2400 CHN elemental analyzer. FTIR spectra were recorded on

College of Chemistry and Material Science, Hebei Normal University, Shijiazhuang, 050024, China. E-mail: hanzg116@126.com

KBr pellets with a FTIR-8900 IR spectrometer in the range of 400-4000 cm^{-1}. TG analysis were performed on a Perkin-Elmer Pyris Diamond TG/DTA instrument in flowing N$_2$ with a heating rate of 10 °C min^{-1}. Powder X-ray diffractions (XRD) were determined by a Bruker AXS D8 Advance diffractometer. UV spectra were measured by U3010 UV-visible spectrophotometer (Shimadzu).

2.2 Preparation of hybrids 1-3

A mixture of MnCl$_2$·4H$_2$O (0.08 g, 0.40 mmol), bpp (0.03 g, 0.15 mmol), Na$_2$MoO$_4$·2H$_2$O (0.24 g, 3.31mmol), H$_3$PO$_4$ (0.5 mL, 7.5 mmol), H$_2$O (8 mL, 0.72 mmol), was stirred for 30 min at room temperature, and pH value was approximately adjusted to 1.2 with NaOH, then the solution was transferred to a Teflon-lined reactor and heated at 160 °C for 5 days. The reactor was cooled to room temperature at a rate of 8 °C h^{-1}. The pale brown crystals of **1** were obtained, washed with distilled water, and air-dried to give a yield of 52% based on Mo. Anal. Calc. for C$_{143}$H$_{264}$Mn$_4$Mo$_{48}$N$_{22}$Na$_6$O$_{262}$P$_{32}$ (%): C, 27.5; H, 2.96; N, 4.92. Found: C, 27.7; H, 2.84; N, 4.97.

Hybrids **2** and **3** were prepared through the similar procedure to that of hybrid **1**, except that the pH values. The mixture was adjusted to *ca*. pH= 2.5 for **2**, and pH= 4.5 for **3** with NaOH solution, respectively. The deep brown–red crystals of **2** (yield: 42% based on Mo) and red block crystals of **3** (yield: 48% based on Mo) were obtained. Elemental anal. calcd (%) for **2** C$_{26}$H$_{62}$Mn$_2$Mo$_{12}$N$_4$Na$_4$O$_{71}$P$_8$ (%): C, 9.24; H, 1.64; N, 1.69; found (%): C, 9.88; H, 1.65; N, 1.78, and for **3** C$_{52}$H$_{92}$Mn$_3$Mo$_{12}$N$_8$Na$_3$O$_{75}$P$_9$ (%): C, 16.54; H, 1.87; N, 3.16; found (%): C, 16.98; H, 1.90; N, 3.05.

2.3 X-ray crystallographic study

Single crystal data were collected on a Smart Apex CCD diffractometer at 296(2) K with Mo *Kα* monochromated radiation (*λ*= 0.71073 Å) at room temperature. The structures of **1-3** were solved by direct methods and refined by the full-matrix least-squares methods on F^2 using the SHELXTL crystallographic software package.[24] Anisotropic thermal parameters were used to refine all non-hydrogen atoms. The positions of hydrogen atoms attached to carbon atoms were fixed at the ideal positions. Hydrogen atoms attached to nitrogen or oxygen atoms were located from the difference Fourier maps and were constrained during the following refinement calculation. A summary of the crystallographic data and structural determination parameters for **1–3** are provided in Supporting Information Table 1. CCDC-1015040 (for **1**), -1015041 (for **2**), -1015042 (for **3**) contain the supplementary crystallographic data for this paper. These data can be obtained free of charge from The Cambridge Crystallographic Data Centre via www.ccdc.cam.ac.uk/data_request/cif.

2.4 Catalytic experiments

The catalytic reactions were carried out in a Pyrex reactor of 80 mL capacity performed. A sample of 20 mg hybrid **1** (**2** or **3**) was dispersed into aqueous solution. Here experiments consist of a systems: K$_3$[Fe(CN)$_6$] (1.0 × 10^{-3} M) and Na$_2$S$_2$O$_3$ (1.3 × 10^{-1} M) solution have been done. The system was magnetically stirred at 50 °C. At 15, 30, 60, 90, 150, 210 min, 3 mL aliquot was sampled and then centrifuged to remove the particles of catalyst. The evolution of absorption spectra due to the reduction of [Fe(CN)$_6$]$^{3-}$ to [Fe(CN)$_6$]$^{4-}$ has been recorded using UV-visible spectrophotometer,

respectively. Spectra of blank experiments in the absence of catalysts were also recorded. To test the reusability of the hybrid, the used catalysts were separated from the solution by centrifuge, and washed, dried, then ready for use in the next cycle. The ionic Equations for the redox reaction are shown in Eq. (1).

$$2S_2O_3^{2-} + 2[Fe(CN)_6]^{3-} \leftrightarrow S_4O_6^{2-} + 2[Fe(CN)_6]^{4-} \qquad (1)$$
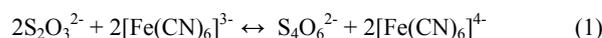
The conversion of Fe(III) was calculated from $([C_0]-[C_i])/C_0 \times$ 100%, where $[C_0]$ is the initial concentration and $[C_i]$ is the concentration at each time point.

3. Results and Discussion

3.1. Structural analysis

Single crystal X-ray diffraction analysis reveals that the basic anionic moiety of hybrids **1-3** all are built upon sandwich-type {P4Mo$_6$X$_{31}$}$^{n-}$ (abbr. {P$_4$Mo$_6$}, X= O or OH) anionic unit. As usually observed, it is made up of six {MoO$_6$} octahedra, four {PO$_4$} tetrahedra and one {MnO$_6$} octahedron linked with corner- and edge-sharing modes. According to the valence bond calculations,[25] all Mo atoms are in the reduced +5 oxidation state (5.140-5.301). P and Mn atoms are +5 and +2 oxidation states (Tables S4-S6), respectively.

The basic composition of hybrid **1** consists of four {Mn[P$_4$Mo$_6$]$_2$} clusters, six [Na(Hbpp)]$^{2+}$, five protonated [H$_2$(bpp)]$^{2+}$ cations, and fourteen lattice water molecules. In {Mn[P$_4$Mo$_6$]$_2$} cluster, the central Mn atom adopts octahedral coordination mode which achieved by three bridging-oxygen atoms between Mo-Mo single bonds of the {Mn[P$_4$Mo$_6$]$_2$} cluster (Fig. 1a). There are two kinds of discrete polyanionic {Mn(P$_4$Mo$_6$)$_2$} units in **1**, labeled as Mn13- and Mn14-containing clusters (Fig. 1b), respectively. The Mn-O bond lengths are of 2.173-2.259 Å. Na$^+$ cations are attached to the surface O atoms of anions via the electrostatic forces, forming a 2D inorganic sheet-like structure (Fig. 1c). All the cationic [Na(Hbpp)]$^{2+}$ units, protonated bpp, PO$_4$$^{3-}$ anions and solvent water molecules reside in the interspaces between two adjacent supramolecular layers via the intermolecular interactions.
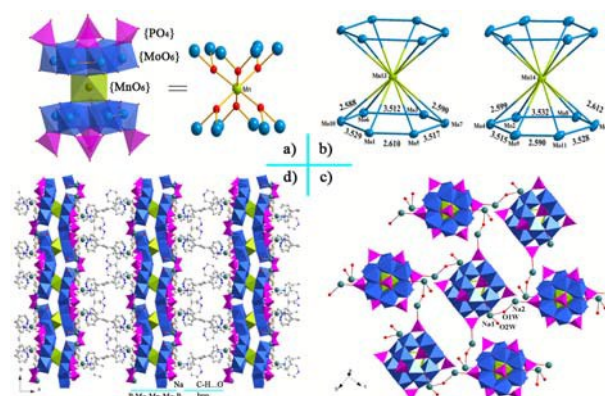
Fig. 1 a) The {Mn(P$_4$Mo$_6$)$_2$} unit in **1**; b) the simplification of six edge-sharing {MoO$_6$} octahedra; c) a polyhedral view showing the 2D inorganic sheet linked through O-Na-OH$_2$-Na-O; d) the 3D supramolecular framework showing the alternative arrangements of inorganic and organic layers through bpp-Na-O and C-H…O linkages.
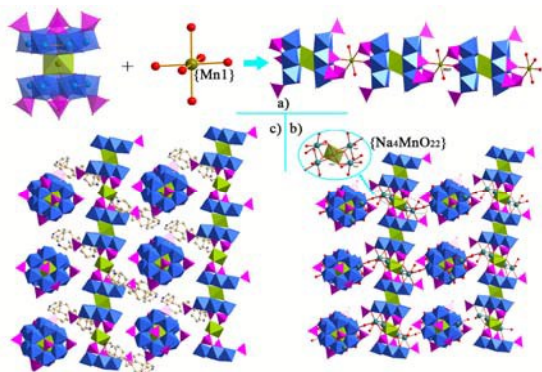
Fig. 2 a) The 1D structure of $\{Mn[Mn(P_4Mo_6)_2]_2\}_\infty$ in **2**; b) a 2D inorganic sheet formed by Na-O interactions; c) the 3D supramolecular framework of **2**.

The component of hybrid **2** consists of a chain-like anionic unit $[Mn(H_2O)_7]\{Mn[Mo_6O_{12}(OH)_3(HPO_4)_3(PO_4)]_2\}^{10-}$, sodium and protonated $[H_2(bpp)]^{2+}$ cations, and water molecules. Mn(2) located at the center of sandwich-type $\{Mn[P_4Mo_6]_2\}$, while Mn1 in the form of $\{Mn(OH_2)_2\}$ fragments bridge $\{Mn[P_4Mo_6]_2\}$ clusters to form a 1-D inorganic extending structure (Fig. 2a). Worthy of mention is that the existence of Na$^+$ ions further stabilizes and extends the inorganic network. As shown in Fig. 2b, four distorted $\{NaO_6\}$ octahedra surround one Mn1 octahedron by edge-sharing mode to form a $\{Na_4MnO_2\}$ unit. In **2**, it could be seen as that the adjacent parallel inorganic chains construct a 2D inorganic sheet; while it is perpendicular each other among chains from adjacent sheets (see Fig. 2c). The protonated bpp and water molecules fill the space formed by the stacking of these inorganic chains.

Similarly, hybrid **3** is composed of $\{Mn[Mo_{12}O_{24}(OH)_6(HPO_4)_6(H_2PO_4)(PO_4)]\}^{8-}$, sodium cation, $[Na_2(bpp)]^{2+}$, $[H(bpp)]^+$, isolated $[HPO_4]^{2-}$ ion and lattice water molecules. The difference is in that these clusters of $\{Mn[P_4Mo_6]_2\}$ are here linked by a double bridge linkages of $\{Mn(OH_2)_2\}_2$ (Mn(1) and Mn(1i)). As shown in Fig. 3, all the adjacent inorganic 1-D chains are parallel with each other to form 2-D inorganic sheets by Na-O linkages, and further the adjacent 2D sheets are also parallel to each other in the same extending directions and finally form the 3D network of **3** through O-Na-bpp-Na-O and hydrogen bonding linkages.
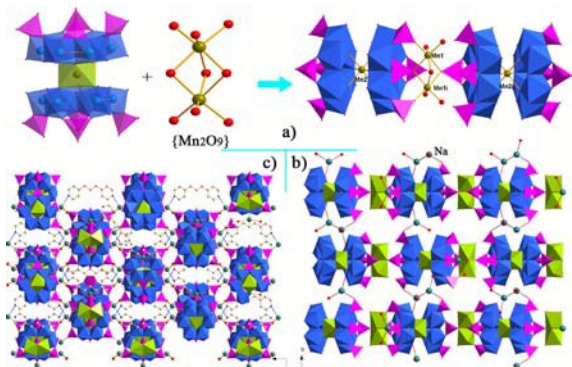
Fig. 3 a) 1D chain-like structure of $\{Mn_2[(P_4Mo_6)_2]\}_\infty$ in **3**; b) 2D inorganic sheet; c) 3D supramolecular framework of **3**. The isolated $[HPO_4]^{2-}$ ion, water molecules and hydrogen atoms are omitted for clarity.

3.2 FT-IR spectra, TG analysis XRD and UV spectra

IR spectra of **1-3** exhibit similar characteristic peaks (see Fig. S1(a-c)). The characteristic bands in the range of 606-745 cm^{-1} are attributed to ν(Mo–O–Mo) vibrations. Strong peaks at 956-966 cm^{-1} are due to ν(Mo=O) vibrations. The ν(P–O) vibration ranges from 1033-1178 cm^{-1}. Strong peaks at 1504-1622 cm^{-1} are assigned to C–C and C–N stretch of organic amines. In addition, broad bands at 3247-3440 cm^{-1} are due to ν(O–H) and ν(N–H). The thermal stabilities are investigated under N_2 atmosphere from 20 to 800 °C. The results show that the main structures of **1-3** are stabilized up to *ca.* 300°C (Fig. S2). The simulated and experimental PXRD patterns of them in the angular region 5-55º are shown in Fig. S3. One can see that the diffraction peaks of both simulated and experimental patterns of **1-3** match in the key positions, respectively, indicating the phase purities of three compounds. The differences in intensity might be due to the preferred orientation of the powder samples. The UV spectra of hybrids **1-3** in methanol have been measured and provided in supporting materials (Fig. S4). One absorption peak at 259 nm in the UV region is assigned to the charge-transfer absorption band of terminal and bridging oxygen atoms to Mo metal atoms.

3.3 Catalytic experiments

The highly reduced structural feature of hybrids **1-3** motivates us to further study their catalytic performance for electron transfer reactions. Catalytic property of hybrids **1-3** have been tested as heterogeneous catalysts for inorganic redox reaction between $Fe(CN)_6^{3-}$ and $S_2O_3^{2-}$ in aqueous solution at room temperature (25 °C) and 50 °C, respectively. For this study, the optical spectra of the respective solutions in presence of catalysts are monitored with respect to time using UV-visible spectrometer. The depletion of the 420 nm peak has been used to study the rate of such a catalyzed reaction, and the results are presented in Fig. 4. It shows the successive UV-vis spectra of the solutions recorded during the redox reaction between $Fe(CN)_6^{3-}$ and $S_2O_3^{2-}$ with a change in color from yellow to light green (see Fig. S5). As shown in the Fig. 4a-c,
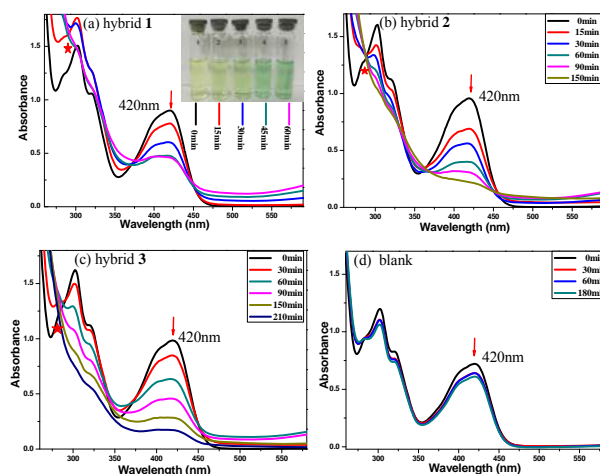
Fig. 4 Successive UV-visible absorption spectra for aqueous solutions of the catalytic reduction reactions of $[Fe(CN)_6]^{3-}$ and $S_2O_3^{2-}$ in the presence of **1**(a), **2**(b), **3**(c). And (d) is the blank experiment without any catalyst at 50 °C.

COMMUNICATION

the depletion of $Fe(CN)_6^{3-}$ peaks have been observed as the reaction proceeding with time in the presence of hybrids **1-3**. For comparisons, the similar tests in the absence of hybrids **1-3** were also performed, and only a very small change of absorption values (see Fig. 4(d)) were observed over a period of 180 min at 50 °C. The results clearly support the catalytic activity of hybrids **1-3** toward the reduction of $[Fe(CN)_6]^{3-}$ to $[Fe(CN)_6]^{4-}$ ions. It may be noted here that the reaction proceeds through a clear isosbestic point at 286 nm, indicating that this redox reaction is proceeding smoothly without forming multiple products. As shown in Fig. 5, the apparent rate constant value is calculated from the slope of the plot of $-\ln A_{420}$ against time to be 1.5×10^{-3} min^{-1} (2.5×10^{-5} s^{-1}) at 25 °C. But, at 50 °C the apparent rate constant value is calculated from the slope to be 8.5×10^{-3} min^{-1} (1.41×10^{-4} s^{-1}), which is five times higher than that obtained at 25 °C. These data are comparable with that the reduction of $[Fe(CN)_6]^{3-}$ in the presence of Au NPs doped mesoporous boehmite films at two temperatures (25°C, 3.12×10^{-3} min^{-1}; 50 °C, 8.43×10^{-3} min^{-1}).[26]

To experimentally verify the reaction observed is truly catalytic process, a blank experiment was designed and performed. The reaction does not occur in absence of such catalysts at those temperatures. There are two kinds of possibilities for the catalytic reduction reaction: i) the reduced POM cluster serves as reductant; ii) the reduced POM cluster serves as catalyst for the reaction of $K_3[Fe(CN)_6]$ and $Na_2S_2O_3$. In order to investigate whether or not surface catalysis takes place, solutions initially containing 1 mM $K_3[Fe(CN)_6]$ were monitored as a function of time in the presence and absence of $Na_2S_2O_3$ and hybrid **1**. Fig. 6 reports the results of these experiments performed in aqueous solution. Curve *a* consists of two stages at 50 °C: the concentration of hexacyanoferrate(III) does not change with the presence of only hybrid **1** under the similar condition during nearly 350 min, indicating without observable hexacyanoferrate(III) absorption onto the surface of **1**. When the reductant $Na_2S_2O_3$ is added, the rapid decrease in $[Fe^{III}]_{aq}$ with the duration of the experiments means that Fe^{III} is quickly transformation to Fe^{II}. These results suggests that hybrid **1** itself can not adsorb as well as not reduce $K_3[Fe(CN)_6]$, but only catalyze the reduction reaction of hexacyanoferrate(III) with $Na_2S_2O_3$; curve *b* indicates that there is a little surface adsorption of Fe^{III} onto crystals at 25 °C, and the maximum adsorption amount is ca. 13.2%. The adsorption process between Fe^{III} and hybrid **1** is slow and the equilibrium is obtain within 250 min; curves *c* and *d*, representing experiments in which both $Na_2S_2O_3$ and hybrid **1** are present at 25 °C and 50 °C, respectively. Combining Fig. 5 and Fig. 6, it is evident that the effect of temperature enhancing catalytic ability is significant under the similar condition. The reason can be ascribed to the increased solvability of hybrids under a higher temperature, leading to a change from a heterogenous to homogeneous process.

Curves *a-b* indicate that it is the crystal surface that serves as catalyst active sites rather than the POM cluster self as reducer. Here, the hybrid **1** has been taken as an example to superficial study the kinetics. The overall catalytic redox reaction may be expressed in Eqs. (1-5). In the derivation, the elementary steps are assumed as below (to simplify the expression, [A] represents $[[Fe(CN)_6]^{3-}]$, [B] represents $[Na_2S_2O_3]$, [*] represents the concentration of vacant active chemisorption sites on the solid catalysts surface, [A*], [B*],
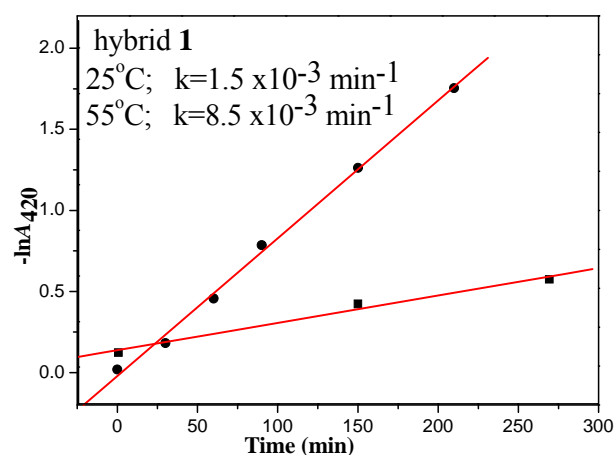
Fig. 5 Pseudo first order plots of $-\ln A$ (absorbance intensity at 420 nm) versus time for the Fe(III) reaction at 25 °C and 50 °C.
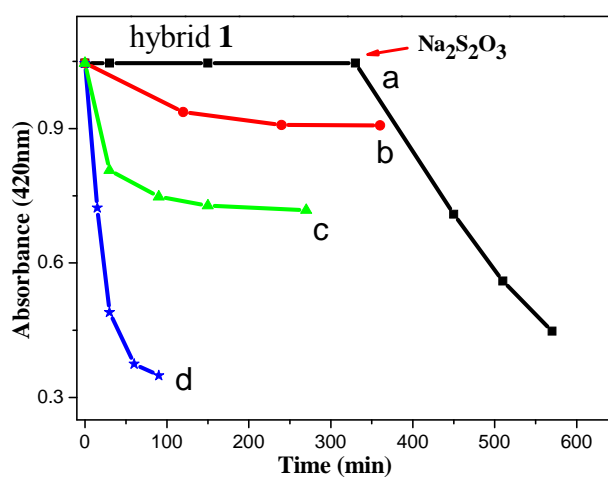
Fig. 6 Reduction of 1 mM Fe(III) by hybrid **1** as a function of time in: (a) $Na_2S_2O_3$-free solution in 350 min and then adding $Na_2S_2O_3$ at 50 °C; (b) $Na_2S_2O_3$-free solution in 350 min at 25 °C; (c) and (d) the presence of both $Na_2S_2O_3$ and **1** at 25 °C and 50 °C, respectively.

(1) $A + * \xleftarrow{K_1} A*$ (step 1: quasi-equilibrated diffusion of A onto surface of crystal)

(2) $B + * \xleftarrow{K_2} B*$ (step 2 : quasi-equilibrated diffusion of B onto surface of crystal)

(3) $A* + B* \xleftarrow{K_3} C* + *$ (step 3 : surface reaction, rate determining step)

(4) $C* + B* \xleftarrow{K_4} P*$ (step 4 : subsequent surface reaction)

(5) $P* \xleftarrow{K_5} P + *$ (step 5 : desorption of product)
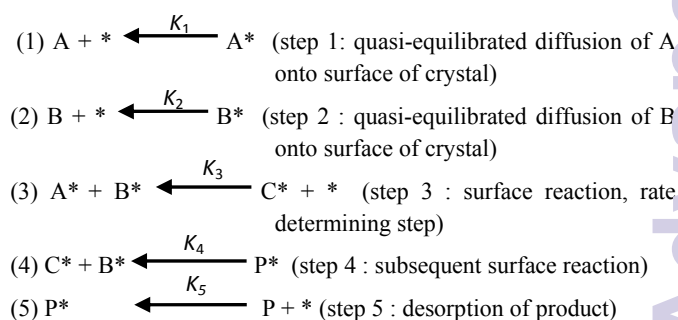
[C*] and [P*] are those of reaction intermediates, and [P] represent the product $[Fe(CN)_6]^{4-}$ ion.[27]

Catalytic property of hybrids **2**, **3** had also been tested as heterogeneous catalysts for this system (see Fig. 7). Additionally, a Keggin-type anion-containing hybrid $(H_2bpp)_2[PMo^{VI}_9Mo^V_3O_{40}]$
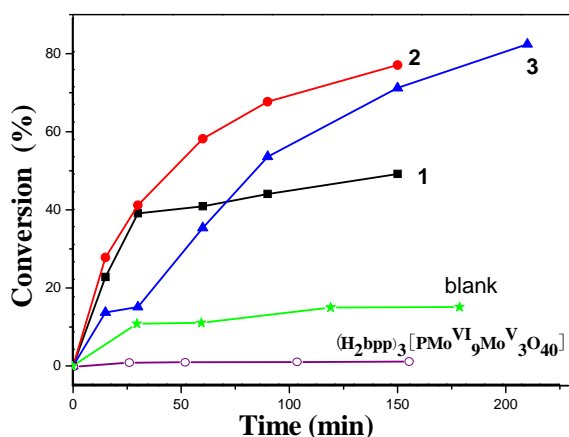
Fig. 7 Plots of conversion Fe(III) vs. time at 50 °C.

with a mixed valence of Mo was conducted as a contrast experiment to check the activity.[28] It is observed that this hybrid is ineffective for the reduction reaction (see Fig. S6). The simple $H_3PMo_{12}O_{40}$ phosphomolybdic acid has not catalytic activity for this system, which is soluble in water and quickly reacts with the reducing agent $Na_2S_2O_3$ to form second pollution heteropoly blue (Fig. S7). Compared to these blank experimental data, hybrids **1**, **2** and **3** show high catalytic activity due to the recombination of inorganic anion $\{P_4Mo_6\}$ and organic bpp. It could be concluded that $\{Mn[P_4Mo_6]_2\}$ cluster in **1-3** play a critical role for this reduction reaction of Fe^{III}, and the extending structural topologies of Mn coordination environment are also related to the catalytic performance. Because the reduction step is an electro-transfer process, reported work also confirmed that the catalysis reaction occurred through the electron transfer at the noble metal NPs surface. Highly reduced polyanion $\{Mn[P_4Mo^V_6]\}$ cluster might be more conducive to electron transfer in a much faster manner.

A POM-based crystalline tubular material IFMC-100 was employed as matrix/microreactor to prepare Au-anchored materials (Au@IFMC-100) by solid–liquid redox reaction. The as-prepared Au@IFMC-100 microtubes exhibit enhanced catalytic performance for the reduction of $K_3Fe(CN)_6$ with $NaBH_4$ in aqueous solution.[29] However, thiosulfate salts are a National Sanitation Foundation (NSF, a WHO collaborator) approved water treatment chemical. The development of a catalytic material that could utilize thiosulfate as the reductant for electron transformation reaction would have significant for environmental benefits.[30] During our course of catalytic experiments, these POM-based supramolecular frameworks maintain higher catalytic activity and structural stability. Importantly, the catalyst can be easily separated after the reaction and resused several times. The catalytic reaction was performed multiple times using the same sample. It is found that the conversion rates of Fe^{3+} become lower with the increase of repeated cycles (see Table 1), which can may be ascribed to that some of crystals are lost with multiple cycles. In addition, a possible reason is that the surface of crystal sample adsorbs a lot of lowly soluble Fe^{2+}, which imped the contact of the catalyst and Fe^{3+} for reducing the catalytic activity. IR spectra of the fresh and used catalysts are measured to check the structural stability of hybrid **1** (Fig. S8). The characteristic peaks illustrate that the skeleton of the parent $\{P_4Mo_6\}$ polyanion still

remains intact after catalytic reaction. Furthermore, X-ray photoelectron spectra are measured to monitor the oxidation state of Mo in hybrid **1** before or after catalysis (see Fig. S9). Two curves for Mo atoms give two peaks at 231.4 and 234.7 eV, attributable to $Mo^{5+}3d_{5/2}$ and $Mo^{5+}3d_{3/2}$, respectively. The results support that Mo^V are stable in its reduced oxidation state (+5) during the catalysis process. The advantages of using such POM hybrid catalysts are therefore many folds: i) the catalysts can be easily separated after the reaction is finished, and be reused after washing with water; ii) the spectra of the solution during the course of catalytic reaction can be monitored without any overlapping absorption originating from the catalyst; iii) these hybrid systems are cheaper and easily obtained, in particularly, they can be structurally designed to optimize their property and application in environmentally friendly catalytic reaction.

Table 1 Catalytic electron transfer (redox) of ferricyanide to ferrocyanide by hybrids **1–3** for different cycles.

	Conversion (%)			
	Fresh	Cycle 1	Cycle 2	Cycle 3
Hybrid **1**	63.5	60.7	53.4	40.0
Hybrid **2**	77.5	71.2	64.5	56.3
Hybrid **3**	81.4	64.6	50.8	46.1

4. Conclusions

In this paper, three reduced molybdophosphate hybrids based on $\{P_4Mo_6\}$ building blocks had been constructed which were tested for the catalytic electron transfer performance of ferricyanide to ferrocyanide. The results indicated that this unique class of hybrids as heterogeneous molecular catalysts has good performance for the electron transfer reaction of hexacyanoferrate (III). The highly catalytic performance of the title hybrids may make them be excellent candidates for catalysis materials of electron transformation reaction. Comparing with noble metal Au/Pt/Pb NPs, the composition of **1-3** is cheaper and easily prepared. Importantly, the catalysts can be easily separated and reused several times. The current work might provide a new idea for exploring POM-based materials in catalytic chemistry. Much work on the hybrids and reaction systems in this field is underway.

Acknowledgements

Supporting Information (see footnote on the first page of this article): Additional IR spectrum, TG curve, PXRD and UV spectra of reaction solutions.

Notes and references

1 I. J. Buerge and S. J. Hug, *Environ. Sci., Technol.*, 1998, **32**, 2092.

2 P. Watts and C. Wiles, *Chem. Commun.*, 2007, 443.

3 B. Deng and A. T. Stone, *Environ. Sci. Technol.*, 1996, **30**, 2484.

4 K. Bhowmik, A. Mukherjee, M. K. Mishra and G. De, *Langmuir*, 2014, **30**, 3209.

5 W. Huang, J. N. Kuhn, C. K. Tsung, Y. Zhang, S. E. Habas, P. Yang and G. A. Somorjai, *Nano Lett.*, 2008, **8**, 2027.

6 B. Lim, M. Jiang, P. H. C. Camargo, E. C. Cho, J. Tao, X. Lu, Y. Zhu and Y. Xia, *Science*, 2009, **324**, 1302.

7 H. L. Jiang, B. Liu, T. Akita, M. Haruta, H. Sakurai and Q. Xu, *J. Am. Chem. Soc.*, 2009, **131**, 11302.

8 X. Huang, P. K. Jain, I. H. El-Sayed and M. A. El-Sayed, *Nanomedicine*, 2007, **2**, 681.

9 J. Sun and X. Bao, *Chem. Eur. J.,* 2008, **14**, 7478.

10 M. Boutros, A. Denicourt-Nowicki, R. A. Alain, L. Gengembre, P. Beaunier, A. Gedeon, and F. Launay, *Chem. Commun.*, 2008, 2920.

11 *Heteropoly, Isopoly Oxometalates.* M. T. Pope, Springer-Verlag: Berlin. 1983.

12 D. L. Long, E. Burkholder and L. Cronin, *Chem. Soc. Rev.*, 2007, **36**, 105.

13 C. Streb, D. L. Long and L. Cronin, *CrystEngComm*, 2006, **8**, 629.

14 K. Yu, W. L. Chen, B. B. Zhou, Y. G. Li, Y. Yu, Z. H. Su, S. Gao and Y. Chen, *CrystEngComm*, 2011, **13**, 3417.

15 X. Zhang, J.Q. Xu and J. H. Yu, *J. Solid State Chem.*, 2007, **180**, 1949.

16 X. Xu, W. W. Ju, D. W. Yan, N. G. Jian and Y. Xu, *J. Coord. Chem.*, 2013, **66**, 2669.

17 Z. G. Han, Y. G. Gao, X. L. Zhai, J. Peng, A. X. Tian, Y. L. Zhao and C. W. Hu, *Cryst. Growth Des.*, 2009, **9**, 1225.

18 X. L. Xue, X. F. Zhao, D. S. Zhang, Z. G. Han, H. T. Yu, X. L. Zhai, *RSC Adv.*, 2014, **4**, 63670.

19 Z. G. Han, X. Q. Chang, J. S. Yan, K. N. Gong, C. Zhao and X. L. Zhai, *Inorg. Chem.*, 2014, **53**, 670.

20 J. S. Yan, X. F. Zhao, J. Huang, K. N. Gong, Z. G. Han and X. L. Zhai, *J. Solid State Chem.*, 2014, **211**, 200.

21 J. S. Yan, K. N. Gong, X. L. Xue, X. L. He, C. Zhao, Z. G. Han and H. T. Yu, *Eur. J. Inorg. Chem.*, 2014, 5969.

22 Z. G. Han, Y. N. Wang, X. J. Song, X. L. Zhai and C. W. Hu, *Eur. J. Inorg. Chem.*, 2011, 3082.

23 K. N. Gong, W. J. Wang, J. S. Yan and Z. G. Han, *J. Mater. Chem. A*, 2015, **3**, 6019.

24 G. M. Sheldrick, SHELXTL-97, *Programs for Crystal Structure Refinement*, University of Göttingen, Germany, 1997.

25 D. Jana, A. Dandapat, G. De, *Langmuir*, 2010, **26**, 12177.

26 I. D. Brown, D. Altermatt, *Sect. B: Struct. Sci.*, 1985, **41**, 244.

27 C. X. Yang, J. H. Meldona, B. Lee and H. Yi, *Catal. Today.*, 2014, **233**, 108.

28 *Crystal data* of $(H_2bpp)_3[PMo^{VI}_9Mo^V_3O_{40}]$: $C_{39}H_{45}Mo_{12}$-$N_6O_{42}P$, Mr= 2452.06, Monoclinic, Space group *Cc*, a = 23.74 (Å), b = 12.68 (Å), c = 22.25(Å); α = 90°, β = 105.81°, γ = 90 °. V = 6408.7 (Å^3), Z = 4, Goodness-of-fit on F^2 1.043, Final R indices [I>2σ(I)], R_1 = 0.0256, wR_2 = 0.0553.

29 D. Y. Du, J. S. Qin, T. T. Wang, S. L. Li, Z. M. Su, K. Z. Shao, Y. Q. Lan, X. L. Wang and E. B. Wang, *Chem. Sci.*, 2012, **3**, 705.

30 A. Pearson and P. O'Mullane, *ChemPlusChem*, 2013, **78**, 1343